

Ceramic-rich composite separators for high-voltage solid-state batteries

Kevin Vattappara^{1,2,3}, Martin Finsterbusch⁴, Dina Fattakhova-Rohlfing^{2,3,4}, Idoia Urdampilleta¹ and Andriy Kvasha^{1,2,*}

¹ CIDETEC, Basque Research and Technology Alliance (BRTA), P. Miramón 196, 20014 Donostia-San Sebastián, Spain; kvattappara@cidetec.es (K.V.); iurdampilleta@cidetec.es (I.U.)

² ALISTORE-European Research Institute, FR CNRS 3104, Hub de l'Énergie, 15 Rue Baudelocque, 80039 Amiens, France; d.fattakhova-rohlfing@fz-juelich.de

³ Faculty of Engineering and Center for Nanointegration Duisburg-Essen CENIDE, Universität Duisburg-Essen, Lotharstraße 1, 47057 Duisburg, Germany

⁴ Institute of Energy Materials and Devices (IMD-2): Materials Synthesis and Processing, Forschungszentrum Jülich GmbH, Wilhelm-Johnen-Straße, 52428 Jülich, Germany; m.finsterbusch@fz-juelich.de

* Correspondence: akvasha@cidetec.es

Keywords: solid state electrolyte; solid state battery; high voltage; composite electrolyte.

1. Synthesis of $\text{Li}_{6.45}\text{Al}_{0.05}\text{La}_3\text{Zr}_{1.6}\text{Ta}_{0.4}\text{O}_{12}$ (LLZO) powder

A modified solid-state reaction (SSR) route was used for the synthesis of LLZO powders used in this work. The synthesis route for aluminum and tantalum doped LLZO powders with nominal composition: $\text{Li}_{6.45}\text{Al}_{0.05}\text{La}_3\text{Zr}_{1.6}\text{Ta}_{0.4}\text{O}_{12}$; has been discussed in detail in an earlier publication [32,60]. The starting powders were stoichiometrically mixed with 10wt% excess Li source to compensate for any loss of Lithium during the sintering step. Precursors used for synthesis: $\text{LiOH}\cdot\text{H}_2\text{O}$ (Applichem-Germany, 99%), La_2O_3 (Merck-Germany, 99.9%, dried for 10 h at 900 °C before start of synthesis), ZrO_2 (Treibacher-Austria, 99.5%), Ta_2O_5 (Treibacher-Austria, 99.99%), and Al_2O_3 (Inframat-Manchester, CT, USA, 99.9%).

In the 1st step, homogenized precursor powders were pressed into pellets of 45 mm diameter and calcined at 850 °C for 20 h in air. In the 2nd and 3rd steps, homogenized powder was calcined at 1000 °C for 20 h in air. Powders were homogenized by milling, then sieved down to <100 µm, and re-pressed into pellets in preparation for next calcination. After the 3rd calcination, pellets were broken, milled and sieved with 100 µm sieve, to prepare for sintering of powders. LLZO powders after calcination, were prepared into pellets with 13 mm diameter for sintering step at 1175 °C for 10 h in air. Sintered pellets were crushed and milled for 1 hour at 100 rpm in a mortar grinder (Retsch RM 200). A scheme of the preparation process has already been reported in our earlier publication [32]. Using a 25 µm standard sieve (CISA - Spain, 200.1 wire mesh-ASTM E-11-2013) synthesized LLZO powder was sieved for preparing C-SCE separators.

2. Synthesis of $\text{Li}_{1.3}\text{Al}_{0.3}\text{Ti}_{1.7}(\text{PO}_4)_3$ (LATP) powder

A modified solution assisted solid-state reaction (SASSR) route was used for the synthesis of LATP powders used in this work. The synthesis route for LATP powders with nominal composition: $\text{Li}_{1.3}\text{Al}_{0.3}\text{Ti}_{1.7}(\text{PO}_4)_3$; has been discussed in detail in an earlier publication by Rosen and colleagues [61]. The starting materials for synthesis: $\text{LiOH}\cdot\text{H}_2\text{O}$ (Applichem-Germany, 99+%), AlPO_3 (Alfa Aesar-Germany, 97%), ZrO_2 (Treibacher-Austria, 99.5%), H_3PO_4 (Alfa Aesar-Germany, 85%), were mixed in stoichiometric amounts in Deionized (DI) water, with $\text{Ti}[\text{OCH}(\text{CH}_3)_2]_4$ (Alfa Aesar-Germany, 97+ %) being added dropwise to the suspension in DI water.

The suspension was mechanically stirred continuously for 4 hours, after which it was kept for drying at 80°C for 7 days. The dried batch of powders were milled and homogenized in a mortar grinder (Retsch RM 200). The homogenized powders were calcined at 600 °C for 5 h in air with heating and cooling rates at 5 °C/min. At the end of calcination step, powder was homogenized by milling, then sieved down to <100 µm, to prepare for sintering of powders. Calcined

LATP powders from the previous step, were prepared as pellets with 13 mm diameter for sintering step at 900 °C for 5 h in air. Sintered pellets were crushed and milled for 1 hour at 100 rpm in a mortar grinder (Retsch RM 200). A scheme of the preparation process is shown below in **Figure S1** below. Using a 25 μm standard sieve (CISA - Spain, 200.1 wire mesh-ASTM E-11-2013) synthesized LATP powder was sieved for preparing C-SCE separators.

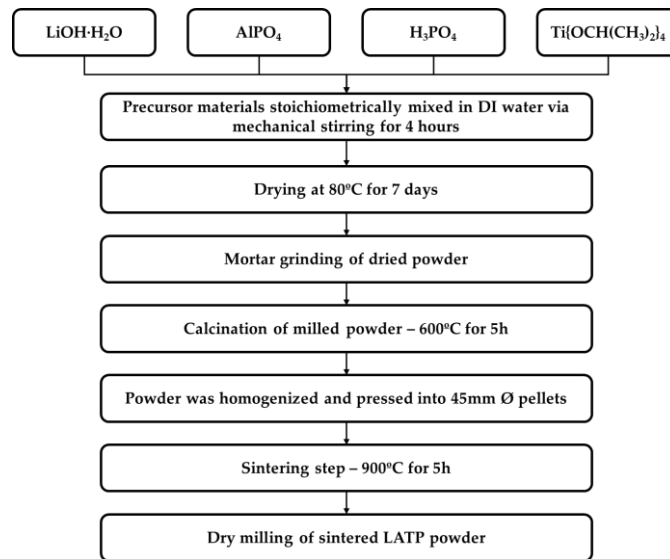


Figure S1. Scheme of LATP synthesis process via solution assisted solid state reaction route.

Figures S2 (a) and **(b)** respectively show XRD diffractogram of the synthesized LLZO and LATP powders. The XRD diffractogram of LLZO in **Figure S2 (a)** shows the conductive cubic phase (space group Ia-3d) [14,62] formation, without any peaks for Li_2CO_3 or Li-deficient $\text{La}_2\text{Zr}_2\text{O}_7$ phases. The XRD diffractogram of LATP in **Figure S2 (b)** shows the conductive rhombohedral phase (space group $R\bar{3}c$) with additional peak for orthorhombic and Al-poor LiTiPO_4 phase each. These additional peaks have already been studied and reported by Rosen et. al [61].

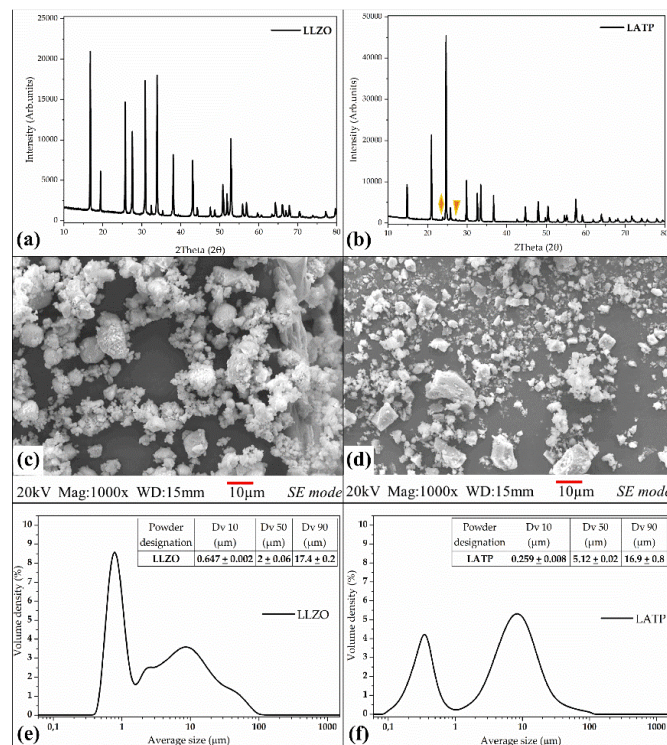


Figure S2. XRD diffractograms of (a) cubic LLZO and (b) rhombohedral LATP powder with (▲) marking additional orthorhombic phase and (▼) marking additional marking additional LiTiPO_5 phase; SEM micrographs for (c) LLZO powder particles and (d) LATP powder particles. Powder particle size distribution graph for (e) LLZO and (f) LATP.

SEM micrographs in **Figure S2** (c) and (d) depict the morphology of LLZO and LATP particles respectively, which are used in this work. **Figure S2** (e) and (f) show the particle size distribution (PSD) for LLZO and LATP powders used in this work. In **Figure S2** (e), the PSD for LLZO particles shows an increased volume density of small particle sizes with a broader distribution peak for medium to big particle sizes with comparatively lesser volume density. On the other hand, LATP powder in **Figure S2** (f), also shows two distinct peaks, however both peaks have similar volume density depicting a bimodal distribution of powder particles.

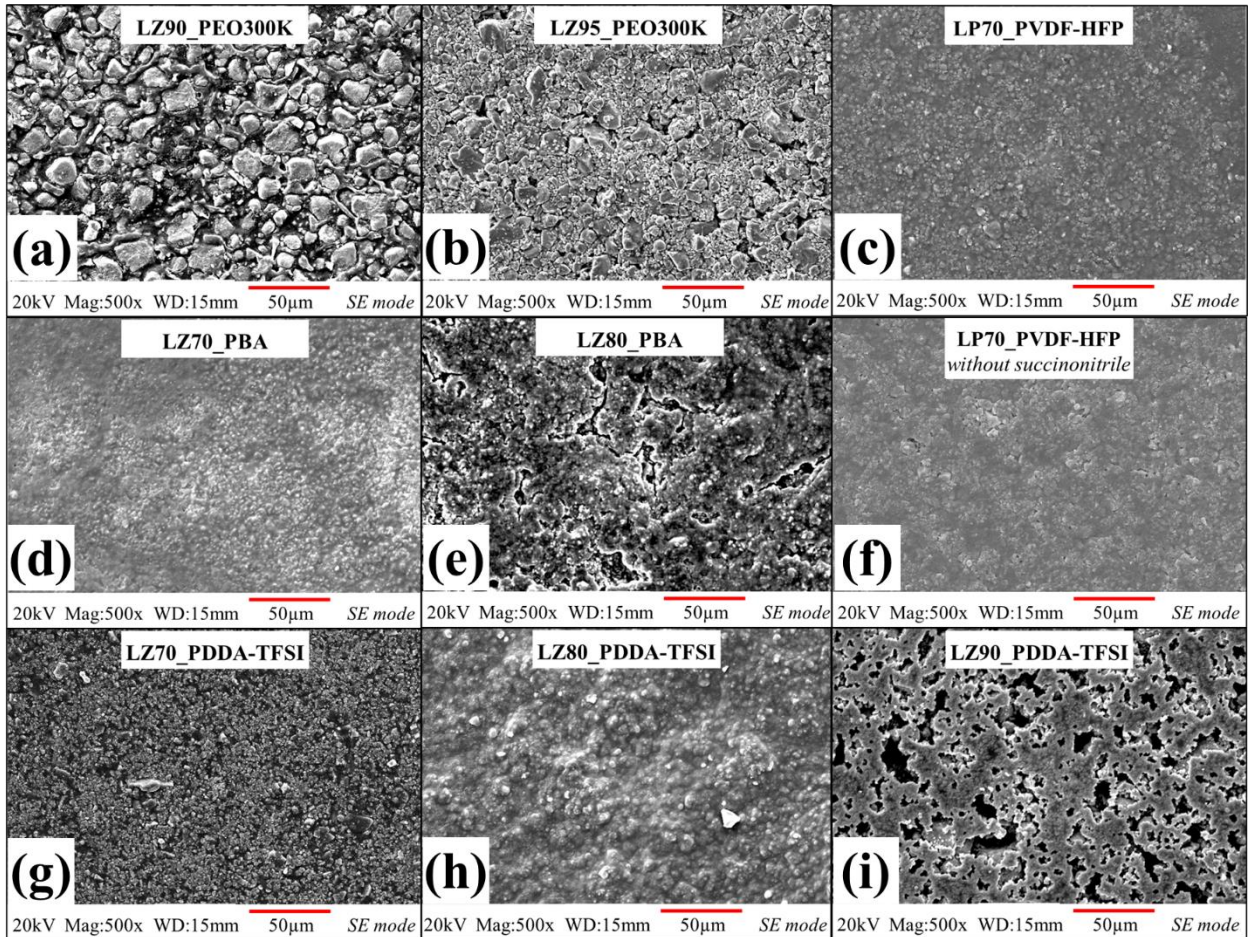


Figure S3. Cross-sectional SEM images of fabricated C-SCEs comparing microstructures of different polymeric matrix groups, starting from PEO matrix based separators [32]: (a) LZ90_PEO300k and (b) LZ95_PEO300k, PVdF-HFP matrix based separators (c) LP70_PVdF-HFP and (f) LP70_PVdF-HFP without SN, PBA matrix based separators (d) LZ70_PBA and (e) LZ80_PBA and PDDA-TFSI matrix based separators (g) LZ70_PDDA-TFSI (h) LZ80_PDDA-TFSI and (i) LZ90_PDDA-TFSI.

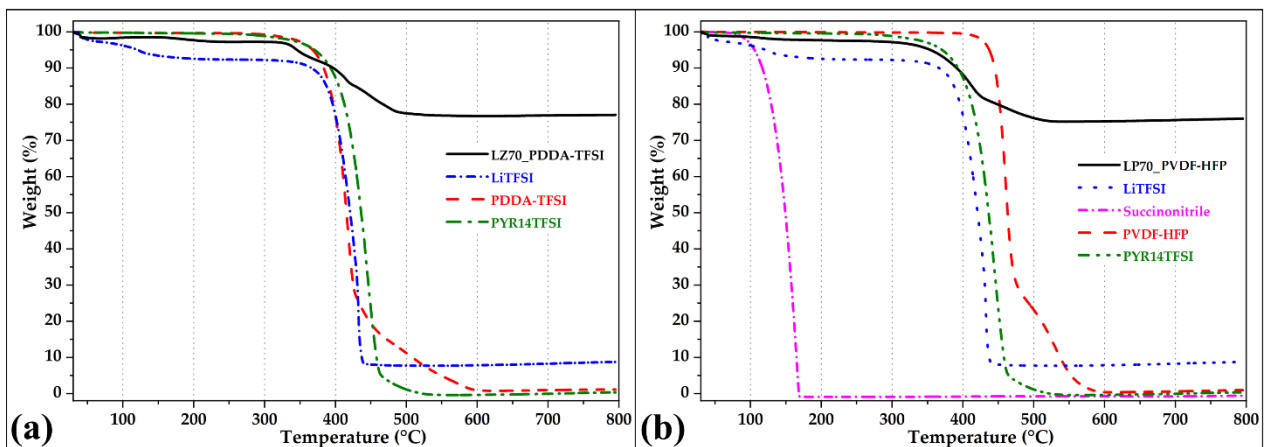


Figure S4. TGA thermographs for (a) LZ70_PDDA-TFSI and (b) LP70_PVdF-HFP.

The determination of Li^+ transference number for GEN 2 C-SCE separators was done by Bruce-Vincent-Watanabe method in symmetric Li/Li cells at 60 °C. More details regarding the measurements can be found in detail in an earlier published work [63].

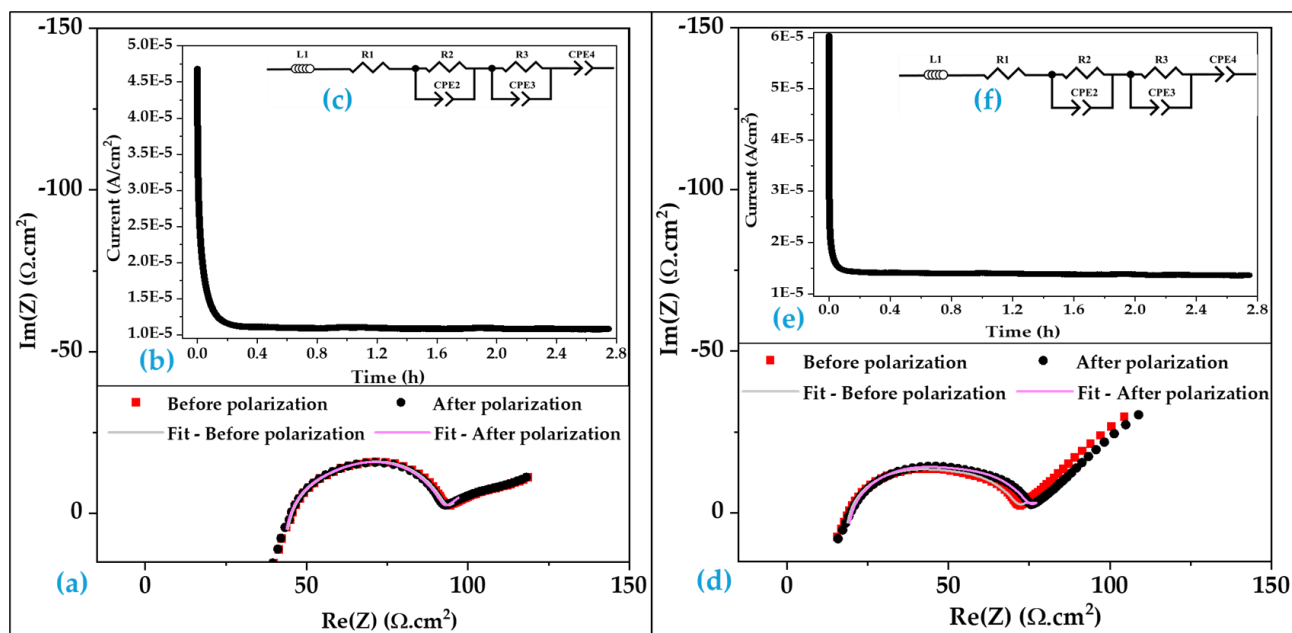


Figure S5. Original and fitted EIS spectra for (a) Li/LZ70_PDDA-TFSI/Li and (d) Li/ LP70_PVdF-HFP /Li cell before and after polarisation; Inset- Chronoamperometry profile (I vs time) of (b) Li/LZ70_PDDA-TFSI/Li and (e) Li/ LP70_PVdF-HFP /Li symmetric cell; (c) and (f) Equivalent circuit used to fit the (before and after polarization) impedance profiles for transference number.

Table S1. Transference number for GEN 2 separators.

C-SCE separators	Transference number (60 °C)
LZ70_PDDA-TFSI	0.13
LP70_PVdF-HFP	0.1

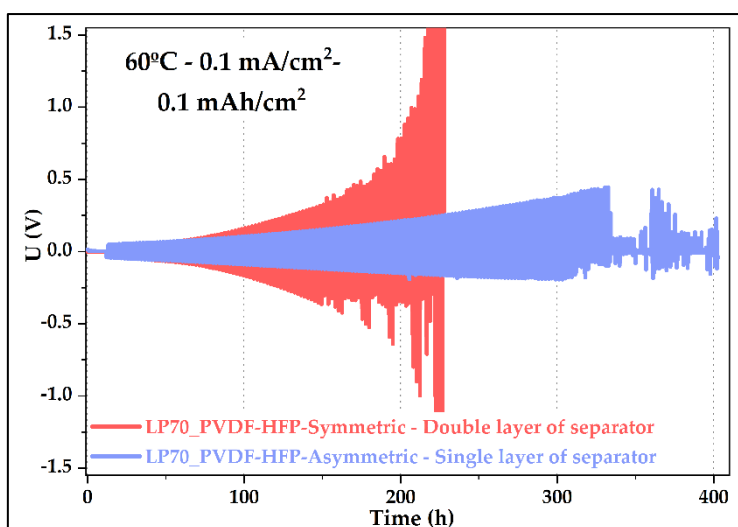


Figure S6. Voltage versus time profiles for long-term galvanostatic cycling of Li/Li cells with LP70_PVdF-HFP. Cycling conditions: current density 0.1 mA/cm², half cycle step of 1 h, 60 °C.

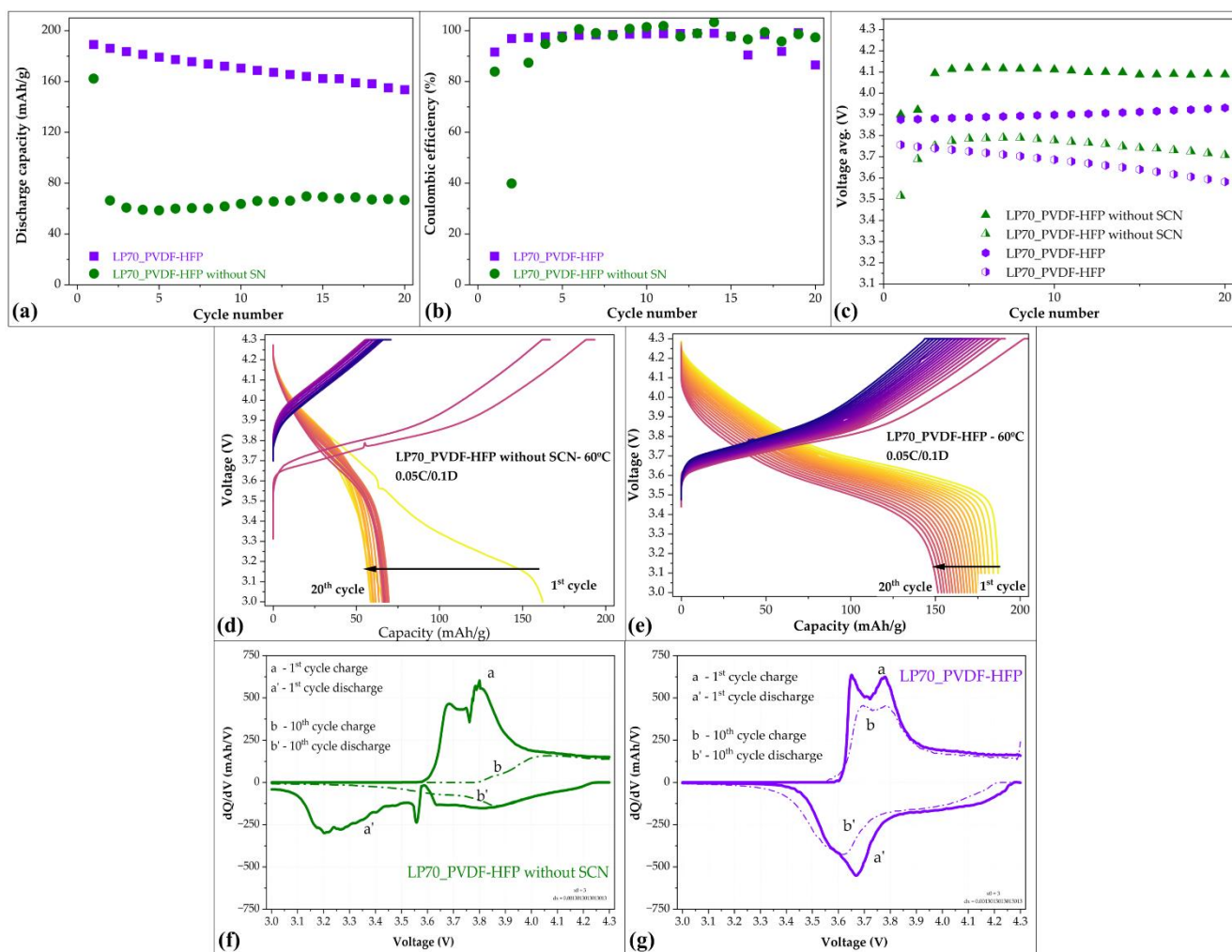


Figure S7. Discharge capacity and (b) coulombic efficiencies efficiency and (c) average voltage of both charge and discharge step of Li/NMC622 cells with LP70_PVdF-HFP and LP70_PVdF-HFP without SCN. Voltage versus capacity curves for Li/NMC622 cells with GEN 2 separators after long-term cycling (d) LP70_PVdF-HFP without SCN and (e) LP70_PVdF-HFP. All comparisons were made after cycling for 20 cycles. dQ/dV versus voltage curves of the 1st and 10th cycles for Li/NMC622 cells with (g) LP70_PVdF-HFP without SCN, (h) LP70_PVdF-HFP.

References

14. Murugan, R.; Thangadurai, V.; Weppner, W. Fast Lithium Ion Conduction in Garnet-Type Li₇La₃Zr₂O₁₂. *Angewandte Chemie International Edition* **2007**, *46*, 7778-7781, doi:https://doi.org/10.1002/anie.200701144.
32. Vattappara, K.; Finsterbusch, M.; Fattakhova-Rohlfing, D.; Kvasha, A. Composite Separators with Very High Garnet Content for Solid-State Batteries. *ChemElectroChem* **2024**, *n/a*, e202400323, doi:https://doi.org/10.1002/celec.202400323.
60. Mann, M.; Küpers, M.; Häuschen, G.; Finsterbusch, M.; Fattakhova-Rohlfing, D.; Guillon, O. The influence of hafnium impurities on the electrochemical performance of tantalum substituted Li₇La₃Zr₂O₁₂ solid electrolytes. *Ionics* **2022**, *28*, 53-62, doi: https://doi.org/10.1007/s11581-021-04300-w.
61. Rosen, M.; Hecker, P.; Mann, M.; Ma, Q.; Gross, J.P.; Schwaiger, R.; Guillon, O.; Fattakhova-Rohlfing, D.; Finsterbusch, M. Reducing the environmental footprint of solid-electrolytes - a green synthesis route for LATP. *Green Chemistry* **2024**, *26*, 2712-2720, doi: https://doi.org/10.1039/D3GC03293K.
62. Tong, X.; Thangadurai, V.; Wachsmann, E.D. Highly conductive Li garnets by a multielement doping strategy. *Inorg Chem* **2015**, *54*, 3600-3607, doi:https://doi.org/10.1021/acs.inorgchem.5b00184.
63. Thieu, T.; Fedeli, E.; Garcia-Calvo, O.; Combarro, I.; Nicolas, J.; Urdampilleta, I.; Kvasha, A. Long cycle-life prototype lithium-metal all-solid-state pouch cells employing garnet-rich composite electrolyte. *Electrochimica Acta* **2021**, *397*, 139249, doi:https://doi.org/10.1016/j.electacta.2021.139249.